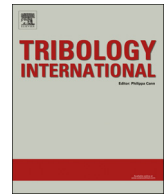




ELSEVIER

Contents lists available at ScienceDirect

Tribology International

journal homepage: www.elsevier.com/locate/triboint

The effect of texture shape on the friction coefficient and stiffness of gas-lubricated parallel slider bearings

Mingfeng Qiu, Bret R. Minson, Bart Raeymaekers*

Department of Mechanical Engineering, University of Utah, Salt Lake City, UT 84112, USA

ARTICLE INFO

Article history:

Received 18 June 2013

Received in revised form

6 August 2013

Accepted 7 August 2013

Available online 20 August 2013

Keywords:

Parallel slider bearings

Hydrodynamic lubrication

Compressible lubricant

Surface texturing

ABSTRACT

Surface texturing is used to increase hydrodynamic pressure and reduce friction and wear between gas-lubricated parallel sliding surfaces in a variety of applications. The shape, geometry, and density of the patterned microtexture features (“dimples”) play a key role in the tribological performance of textured slider bearings. In this paper we evaluate the friction coefficient and stiffness of gas-lubricated textured parallel slider bearings as a function of six different texture shapes. The texture geometry and density are optimized in terms of minimum friction coefficient and maximum bearing stiffness for each individual texture shape, and then compared relative to each other. The ellipsoidal shape is found to yield the minimum friction coefficient and the highest bearing stiffness, independent of the operating conditions.

© 2013 Elsevier Ltd. All rights reserved.

1. Introduction

Enhancing the tribological performance of two surfaces in relative motion is of primary importance in developing mechanical systems with, for instance, increased durability and energy efficiency. Friction force and wear increase dramatically when surfaces interact without the benefit of a lubricant film separating them. Surface texturing can be used to form micro- or nanoscale cavities or pockets (typically called “dimples”) in an arrayed pattern on one of the sliding surfaces. Several fabrication techniques can be used to manufacture this type of texture, such as vibro-rolling [1], reactive ion etching [2], abrasive jet machining [3], LIGA [4], vibromechanical texturing [5] and laser surface texturing [6]. Experimental results indicate that surface texture acts like miniature hydrodynamic bearings and generate a net pressure increase in the thin lubricant film separating the sliding surfaces. This additional pressure increases the separation between the sliding surfaces and correspondingly reduces friction and wear. Applications of surface texturing include mechanical seals [7], gas seals [8,9], thrust bearings [10,11], journal bearings [12], piston rings [13], magnetic tape guides [14,15] and hydraulic systems [16]. While several publications report on the increased load carrying capacity of textured bearings [10,17,18], limited information is available on the effect of different surface texture shapes and geometries on the bearing stiffness and the friction coefficient between the bearing surfaces.

Most experimental studies concerning the friction coefficient of textured bearings only explore a limited range of texture geometries using an incompressible lubricant [3,4,19,20]. Wakuda et al. [3] tested steel pins sliding on textured ceramic plates and suggested that the reduction of the friction coefficient greatly depends on the size and density of the texture features. Stephens et al. [4] used a LIGA process to create a micro-asperity texture on a surface and measured sliding friction against different specimens. They concluded that the geometry of the asperity texture can be optimized to greatly reduce the friction coefficient. Modeling work has also mostly focused on (incompressible) liquid lubricated bearings [21–25]. Sahlin et al. [24] solved the Navier–Stokes equations to optimize the geometry and shape of a single groove on a surface, to maximize load carrying capacity and minimize the friction coefficient. The same approach was used by Cupillard et al. [21] to find the optimal texture depth and density of spherical texture shapes, and minimize the friction coefficient in a journal bearing. Pascovici et al. [25] analyzed a one-dimensional partially textured parallel slider bearing by directly solving the Reynolds equation. They found that the optimal texture geometries for maximum load carrying capacity and minimum friction coefficient are almost identical. Siripuram and Stephens [26] studied concave dimples with seven different shapes and investigated the effect of texture density on the friction coefficient between bearing surfaces separated by an incompressible lubricant. They concluded that the texture density rather than the texture shape is critical to reduce the friction coefficient. However, the depth of different texture shapes was kept constant in their study, potentially preventing each shape from reaching its optimal geometry, since the optimum for different geometries and/or shapes may not necessarily be achieved for a constant dimple depth.

* Corresponding author. Tel.: +1 8015857594.

E-mail address: bart.raeymaekers@utah.edu (B. Raeymaekers).

Nomenclature

a, b	half-length of the ellipse axis in the x - and y -direction, respectively
c	minimum bearing spacing
c_{eq}	equivalent minimum bearing spacing
f	friction coefficient
$H(X, Y)$	non-dimensional local bearing spacing, $H(X, Y) = h(x, y)/c$
$h(x, y)$	local bearing spacing
h_{eq}	equivalent texture depth
h_p	texture depth
K	area ratio; ratio of length of inner and outer equilateral triangles forming the chevron shape, with $0 \leq K \leq 1$
k	non-dimensional bearing stiffness
l	length of the edge of the outer triangle defining the chevron shape
$P(X, Y)$	non-dimensional local bearing pressure, $P = p(x, y)/p_0$
$p(x, y)$	local bearing pressure
p_0	atmospheric pressure

p_{avg}	average bearing pressure
r_1	half-length of the square unit cell
r_p	characteristic radius of the texture
S_p	texture density
U	relative sliding velocity
X, Y	non-dimensional Cartesian coordinates, $X = x/r_p$, $Y = y/r_p$
x, y, z	Cartesian coordinates
δ	non-dimensional minimum bearing spacing, $\delta = c/2r_p$
δ_{eq}	equivalent non-dimensional minimum bearing spacing, $\delta_{eq} = c_{eq}/2r_p$
ε	texture aspect ratio for spherical, circular, triangular and chevron texture shapes, $\varepsilon = h_p/2r_p$
$\varepsilon_1, \varepsilon_2$	texture aspect ratios for ellipsoidal and elliptical texture shapes, $\varepsilon_1 = h_p/2a$, $\varepsilon_2 = h_p/2b$
λ	flow factor, $\lambda = 3\mu U/2r_p p_0$
μ	gas dynamic viscosity
τ	average shear stress in the lubricant film
$\bar{\tau}$	non-dimensional average shear stress in the lubricant film, $\bar{\tau} = \tau/p_0$

Other studies have dealt with compressible lubricants. Murthy et al. [27] solved the compressible Reynolds equation with rarefaction effects to analyze an inclined plane slider bearing textured with spherical dimples. They found that the stiffness of the compressible lubricant film increased with decreasing clearance of the inclined plane slider bearing, but they did not address the relationship between texture geometry, texture shape and bearing stiffness. Raeymaekers et al. [15] demonstrated the effectiveness of surface texturing to reduce the friction coefficient between a cylindrical guide surface and a magnetic tape in magnetic tape drives. They also briefly discussed the non-linear stiffness of the textured gas bearing. Finally, Feldman et al. [28] simulated a partially textured hydrostatic gas bearing and optimized the geometry of spherical dimples for maximum bearing stiffness. Their results suggest that the geometry of the texture has a significant effect on the bearing performance.

No systematic study detailing the effect of texture shape and geometry on the friction coefficient and stiffness of textured parallel gas bearings appears to exist in the open literature. Previous studies are focused on one specific texture shape [28], or constrain one or more geometric parameters when comparing the tribological performance of different texture shapes [17,26], thus, not comparing the optimized geometries of different texture shapes. In a previous paper [18], we have optimized the load carrying capacity for six different texture shapes without constraining the texture geometry, and we have compared the results relative to each other. The ellipsoidal texture shape was found to result in the maximum load carrying capacity. However, while of critical importance in bearing design, the effect of texture shape on the friction coefficient and the bearing stiffness has not yet been examined. Therefore, the objective of this paper is to perform a systematic study of the effect of texture shape and geometry on the friction coefficient and the stiffness of gas-lubricated parallel slider bearings.

2. Methods

2.1. Analytical model

Fig. 1 shows a schematic of the model of a textured parallel slider bearing. The compressible, steady-state Reynolds equation is solved over a domain covering a column of ten dimples, identical to [18]. Only full texturing is considered. Each dimple is centered in a square

unit cell of width $2r_1$. The following assumptions are made: (1) the dimples are identical in shape (for instance, ellipsoidal). (2) The lubricant is air at room temperature, and inertial effects are neglected because the relative velocity and the minimum spacing between the two sliding surfaces are small [29]. The minimum spacing is large enough to neglect rarefaction effects and slip occurring at the solid boundary. (3) Hydrodynamic lubrication is assumed and no asperity contact exists. With these assumptions the steady-state two-dimensional compressible Reynolds equation is given as

$$\frac{\partial}{\partial x} \left(p h^3 \frac{\partial p}{\partial x} \right) + \frac{\partial}{\partial y} \left(p h^3 \frac{\partial p}{\partial y} \right) = 6\mu U \frac{\partial (p h)}{\partial x}, \quad (1)$$

where x and y represent the Cartesian coordinates shown in Fig. 1. $p(x, y)$ is the local bearing pressure, $h(x, y)$ is the local clearance between sliding surfaces, μ is the dynamic viscosity of air, and U is the relative sliding velocity between the two surfaces. Eq. (1) can be written in non-dimensional form as

$$\frac{\partial}{\partial X} \left(P H^3 \frac{\partial P}{\partial X} \right) + \frac{\partial}{\partial Y} \left(P H^3 \frac{\partial P}{\partial Y} \right) = \frac{\lambda}{\delta^2} \frac{\partial (P H)}{\partial X}, \quad (2)$$

with $X = x/r_p$, $Y = y/r_p$, $P(X, Y) = p(x, y)/p_0$ and $H(X, Y) = h(x, y)/c$. p_0 denotes the atmospheric pressure, c is the minimum bearing spacing, and r_p is

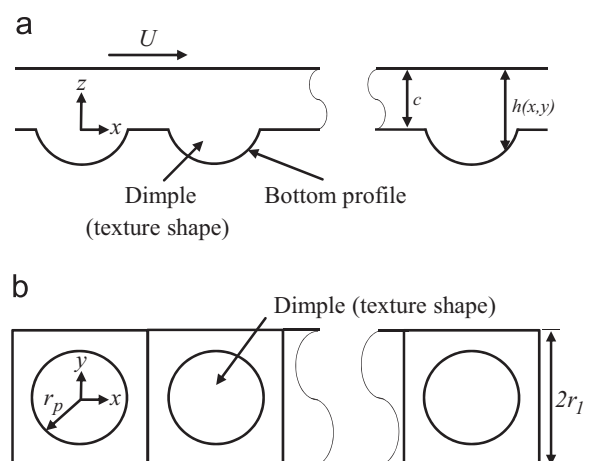


Fig. 1. Model of a textured parallel slider bearing showing (a) a cross-sectional view of a column of dimples, and (b) top view.

the characteristic radius of the texture shape (see Figs. 1 and A1). The operating conditions for the simulation are expressed by the flow factor $\lambda = 3\mu U/2r_p p_0$ and the minimum spacing in non-dimensional form $\delta = c/2r_p$. Atmospheric pressure is maintained at the inlet and outlet of the solution domain. The presence of adjacent dimples in the span-wise flow direction (lateral edge) is accounted for with symmetric boundary conditions, i.e.,

$$P\left(-\frac{r_1}{r_p}, Y\right) = P\left(\left(N - \frac{1}{2}\right)\frac{2r_1}{r_p}, Y\right) = 1, \tag{3a}$$

$$\frac{\partial P}{\partial Y}\left(X, -\frac{r_1}{r_p}\right) = \frac{\partial P}{\partial Y}\left(X, \frac{r_1}{r_p}\right) = 0, \tag{3b}$$

where N represents the number of unit cells in the column of dimples, and r_1 is half the width of a unit cell (see Fig. 1). Eqs. (2), (3a) and (3b) are solved numerically using the finite difference method with central discretization on a staggered grid, and with an over-relaxation factor of 1.4. An error criterion of 0.01% change of pressure at each node between iterations is used to ensure convergence.

2.2. Friction coefficient and bearing stiffness

The friction in the air bearing operating in the hydrodynamic lubrication regime is entirely driven by the shear stress in the lubricant film. The average shear stress is approximated as

$$\tau = \frac{\mu U}{c_{eq}}, \tag{4}$$

where c_{eq} is the equivalent minimum bearing spacing, defined as

$$c_{eq} = c + h_{eq}. \tag{5}$$

c represents the minimum bearing spacing (see Fig. 1), and h_{eq} is the equivalent texture depth, calculated as the volume of a dimple divided by the area of its unit cell, $(2r_1)^2$. The extra bearing spacing due to the presence of the texture is thus averaged over the entire bearing

surface. This treatment captures the global effect of reducing the friction coefficient by means of the texture on an average level, and effectively predicts the magnitude and trend of the friction coefficient as demonstrated in [15]. A more sophisticated model could include calculating the local shear stress from the strain rate near the sliding surface based on the solution of the Reynolds equation, but the former method is used since simplicity is preferred here. When defining $\delta_{eq} = c_{eq}/2r_p$, Eq. (4) can be re-written in non-dimensional form as

$$\bar{\tau} = \frac{\lambda}{3\delta_{eq}}, \tag{6}$$

where $\bar{\tau} = \tau/p_0$. Finally, the friction coefficient f can be expressed as the ratio of the shear stress and the average bearing pressure,

$$f = \frac{\tau}{p_{avg} - p_0} = \frac{\bar{\tau}}{P_{avg} - 1}. \tag{7}$$

The stiffness of the air bearing is defined as the derivative of the load carrying capacity with respect to the bearing spacing, or in non-dimensional form,







$$k = \frac{\partial(P_{avg} - 1)}{\partial \delta}, \tag{8}$$

where the load carrying capacity is expressed as the non-dimensional average gauge pressure. To calculate k , the Reynolds equation is solved to find the average gauge pressure as a function of bearing spacing δ , and the slope of the curve is determined in a discrete set of points by a central finite difference scheme.

2.3. Comparison of different texture shapes

Six different, commonly used texture shapes are evaluated, including four shapes with a flat bottom profile; circular, elliptical, triangular and chevron texture shapes, and two shapes with a curved bottom profile; spherical and ellipsoidal. The non-dimensional parameters to describe the texture geometries are

Table 1
Texture shape, texture geometry parameters and the equations used to optimize the texture geometries (a, b are semi-axes length of the elliptical contour parallel and perpendicular to the flow direction, respectively; K is the ratio of the size of the inner triangle and outer triangle forming the chevron shape (Appendix A and [18])).

Texture shape	Bottom profile	Non-dimensional parameters	Equivalent spacing equations (1) h_{eq} (2) δ_{eq}
Circle 	Flat	$\epsilon = \frac{h_p}{2r_p}, S_p = \frac{\pi r_p^2}{4r_1^2}$	(1) $h_{eq} = \frac{\pi r_p^2 h_p}{4r_1^2}$ (2) $\delta_{eq} = \delta + \epsilon S_p$
Sphere 	Curved		(1) $h_{eq} = \frac{\pi h_p}{4r_1^2} \left(\frac{h_p^2}{6} + \frac{r_p^2}{2} \right)$ (2) $\delta_{eq} = \delta + \frac{2}{3} \epsilon S_p \left(\epsilon^2 + \frac{3}{4} \right)$
Ellipse 	Flat	$\epsilon_1 = \frac{h_p}{2a}, \epsilon_2 = \frac{h_p}{2b}, S_p = \frac{\pi r_p^2}{4r_1^2} = \frac{\pi ab}{4r_1^2}$ a, b : Semi-axes of the ellipse/ellipsoid	(1) $h_{eq} = \frac{\pi ab h_p}{4r_1^2}$ (2) $\delta_{eq} = \delta + S_p \sqrt{\epsilon_1 \epsilon_2}$
Ellipsoid 	Curved		(1) $h_{eq} = \frac{\pi ab h_p}{4r_1^2} \left(\frac{h_p^2}{6b^2} + \frac{1}{2} \right)$ (2) $\delta_{eq} = \delta + \frac{2}{3} S_p \sqrt{\epsilon_1 \epsilon_2} \left(\epsilon_2^2 + \frac{3}{4} \right)$
Triangle 	Flat	$\epsilon = \frac{h_p}{2r_p}, S_p = \frac{3\sqrt{3}r_p^2}{16r_1^2}$	(1) $h_{eq} = \frac{3\sqrt{3}r_p^2 h_p}{16r_1^2}$ (2) $\delta_{eq} = \delta + \epsilon S_p$
Chevron 	Flat	$\epsilon = \frac{h_p}{2r_p}, K, S_p = \frac{3\sqrt{3}(1-K^2)r_p^2}{16r_1^2}$	(1) $h_{eq} = \frac{3\sqrt{3}r_p^2 h_p (1-K^2)}{16r_1^2}$ (2) $\delta_{eq} = \delta + \epsilon S_p$

the texture aspect ratio ε , defined as the ratio of the depth and the characteristic diameter of the texture feature, and the texture density S_p , defined as the ratio of the area covered by the texture and the total area of a unit cell. Two texture aspect ratios, ε_1 and ε_2 , are used for elliptical and ellipsoidal shapes, and an area ratio K is used for the chevron shape (see Appendix A and [18]). All texture shapes with the non-dimensional parameters describing their geometry and corresponding equivalent spacing are summarized in Table 1. The operating conditions in this study are fixed as $\delta=0.002$ and $\lambda=2.0 \times 10^{-5}$, conditions relevant to several bearing applications including magnetic tape drives. For each texture shape, the friction coefficient and bearing stiffness are calculated for a range of different geometries (ε , S_p) from the numerical solution of the Reynolds equation. The optimized texture geometries resulting in minimum friction coefficient and maximum bearing stiffness, respectively, are identified from the numerical results for each texture shape and compared relative to each other.

3. Optimization of the geometry of individual texture shapes

3.1. Circular, spherical and triangular texture shapes

Figs. 2, 3 and 4 display the friction coefficient as a function of texture density for different values of the texture aspect ratio, for

the circular, spherical, and triangular texture shapes, respectively. Additionally, Figs. 5, 6 and 7 depict the corresponding non-dimensional bearing stiffness as a function of texture density for different values of the texture aspect ratio for the same texture shapes. In each figure, an optimal texture geometry (ε and S_p)

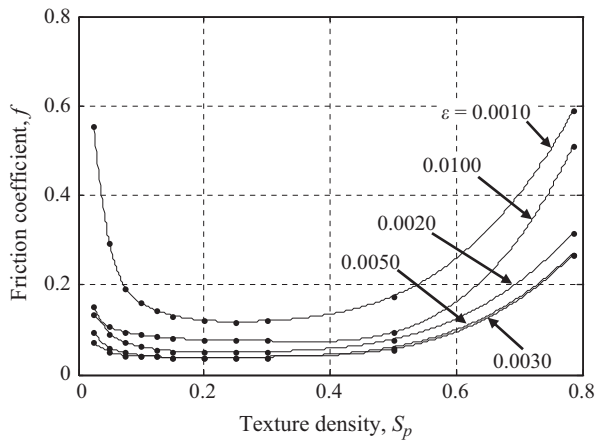


Fig. 2. Friction coefficient as a function of texture density for different values of the texture aspect ratio, for the case of the circular texture shape. $\delta=0.002$ and $\lambda=2.0 \times 10^{-5}$.

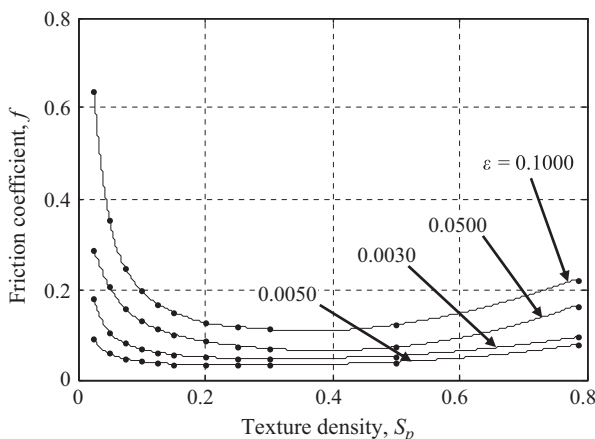


Fig. 3. Friction coefficient as a function of texture density for different values of the texture aspect ratio, for the case of the spherical texture shape. $\delta=0.002$ and $\lambda=2.0 \times 10^{-5}$.

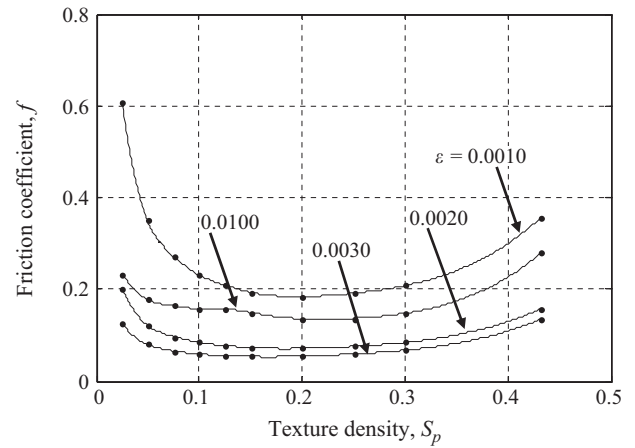


Fig. 4. Friction coefficient as a function of texture density for different values of the texture aspect ratio, for the case of the triangular texture shape. $\delta=0.002$ and $\lambda=2.0 \times 10^{-5}$.

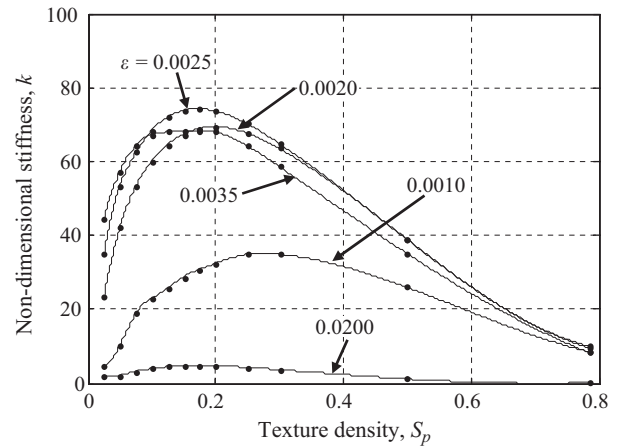


Fig. 5. Non-dimensional stiffness as a function of texture density for different values of the texture aspect ratio, for the case of the circular texture shape. $\delta=0.002$ and $\lambda=2.0 \times 10^{-5}$.

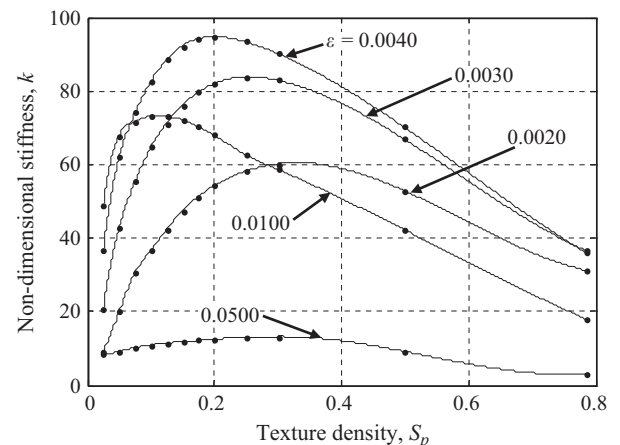


Fig. 6. Non-dimensional stiffness as a function of texture density for different values of the texture aspect ratio, for the case of the spherical texture shape. $\delta=0.002$ and $\lambda=2.0 \times 10^{-5}$.

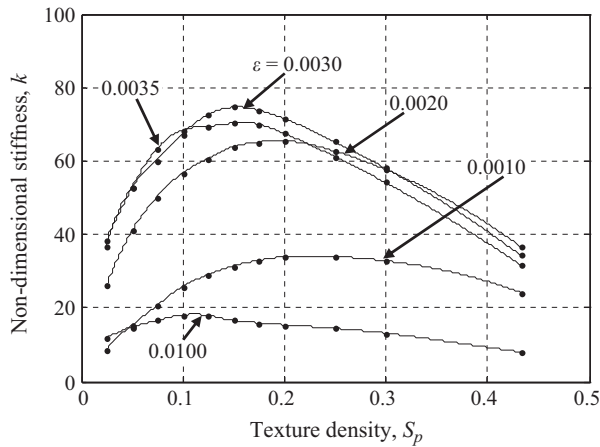


Fig. 7. Non-dimensional stiffness as a function of texture density for different values of the texture aspect ratio, for the case of the triangular texture shape. $\delta=0.002$ and $\lambda=2.0 \times 10^{-5}$.

exists for minimum friction coefficient or maximum bearing stiffness, respectively. For each individual texture shape, the friction coefficient first decreases and then increases with increasing texture density, for a constant texture aspect ratio. For a small value of the texture density (e.g., $S_p < 0.05$), the load carrying capacity and the equivalent bearing spacing δ_{eq} are small, which increases the shear stress in the lubricant and, thus, increases the friction coefficient. When the texture density exceeds $S_p=0.150$, which generates the highest load carrying capacity [18], the friction coefficient remains low until approximately $S_p=0.300$. This is due to the increasing dimple volume with increasing S_p and, thus, increasing δ_{eq} and decreasing shear stress. When further increasing the texture density, the friction coefficient increases again as a result of the significantly reduced load carrying capacity of textured bearings with $S_p > 0.300$. The effect of texture density on bearing stiffness is directly correlated to the change of the load carrying capacity, because a higher load carrying capacity requires a larger pressure increase to change the bearing spacing. For circular texture shapes, the minimum friction coefficient is 0.0371 with $S_p=0.200$ and $\epsilon=0.0030$, and the maximum non-dimensional bearing stiffness is 74.29 with $S_p=0.175$ and $\epsilon=0.0025$. For spherical texture shapes, the minimum friction coefficient is determined as 0.0323 with $S_p=0.250$ and $\epsilon=0.0050$, and the maximum non-dimensional bearing stiffness is 99.05 with $S_p=0.175$ and $\epsilon=0.0060$. For triangular texture shapes, the minimum friction coefficient is 0.0534 with $S_p=0.150$ and $\epsilon=0.0030$, and the maximum non-dimensional bearing stiffness is 74.65 with $S_p=0.150$ and $\epsilon=0.0030$. We note that the geometries for minimum friction coefficient and maximum bearing stiffness are not identical. This will be further discussed in Section 4 of this paper.

3.2. Elliptical and ellipsoidal texture shapes

The elliptical texture shape requires two texture aspect ratios, ϵ_1 and ϵ_2 , to fully define the geometry (see Table 1). Fig. 8 shows the friction coefficient as a function of the texture aspect ratios for the elliptical texture shape, for $S_p=0.175$, 0.350 and 0.500, respectively. The S_p values presented here minimize the friction coefficient ($S_p=0.350$), and additionally display one case on either side of this optimum ($S_p=0.175$, 0.500). The range of possible combinations of ϵ_1 and ϵ_2 is theoretically constrained because an elliptical/ellipsoidal texture shape cannot achieve an arbitrarily large or small ϵ_1/ϵ_2 ratio without extending beyond the unit cell for a specific texture density [18], which is denoted by the solid straight lines. For each value of the texture density, an optimal combination of ϵ_1 and ϵ_2 exists that minimizes the friction coefficient. The optimum is found to be

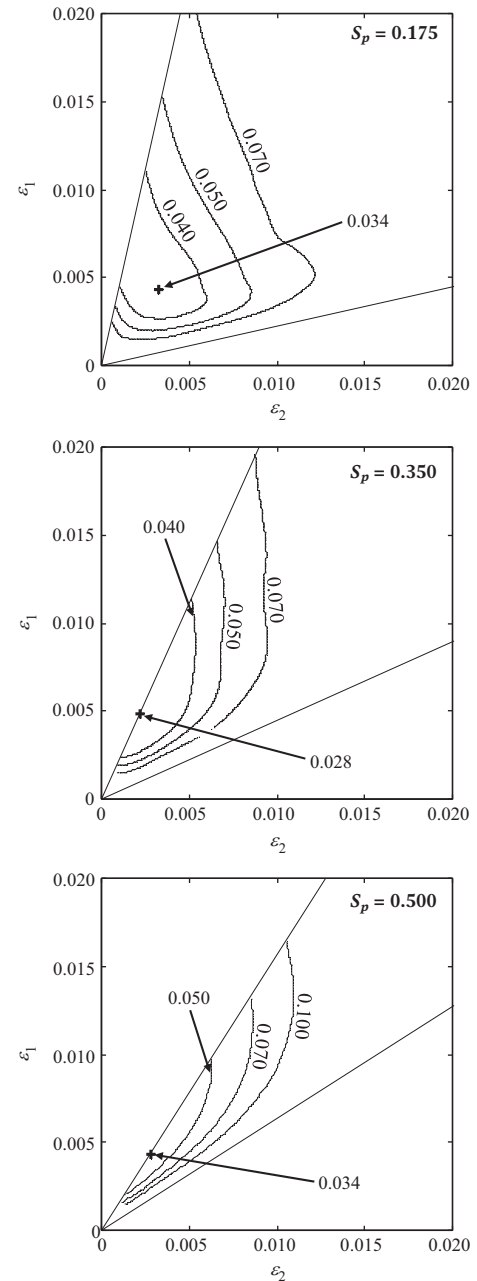


Fig. 8. Friction coefficient as a function of different texture aspect ratio combinations ϵ_1 and ϵ_2 for $S_p=0.175$, 0.350 and 0.500, for the case of the elliptical texture shape. $\delta=0.002$ and $\lambda=2.0 \times 10^{-5}$. The optimum for each texture density is indicated by "+". The range of combinations of ϵ_1 and ϵ_2 that constrains the dimple within the unit cell is denoted by solid lines.

$f=0.0279$ with $S_p=0.350$ and $\epsilon_1=0.0048$, $\epsilon_2=0.0021$. With increasing texture density the texture geometry that minimizes the friction coefficient first stretches along the axis orthogonal to the flow direction to take full advantage of compressing the lubricant flow, thus placing the longitudinal axis orthogonal to the flow. For a specific S_p the optimal geometry reaches the lateral edge of the unit cell and, when further increasing S_p , the geometry must stretch in the direction of the flow, which is similar to what we found in [18]. Fig. 9 displays the non-dimensional bearing stiffness as a function of the texture aspect ratios for the elliptical texture shape, for $S_p=0.175$, 0.350 and 0.500. The optimal texture geometry for maximum bearing stiffness is $S_p=0.350$ and $\epsilon_1=0.0029$, $\epsilon_2=0.0013$, resulting in $k=90.67$. Figs. 10 and 11 present the friction coefficient and bearing stiffness as a function of the texture aspect ratios for the

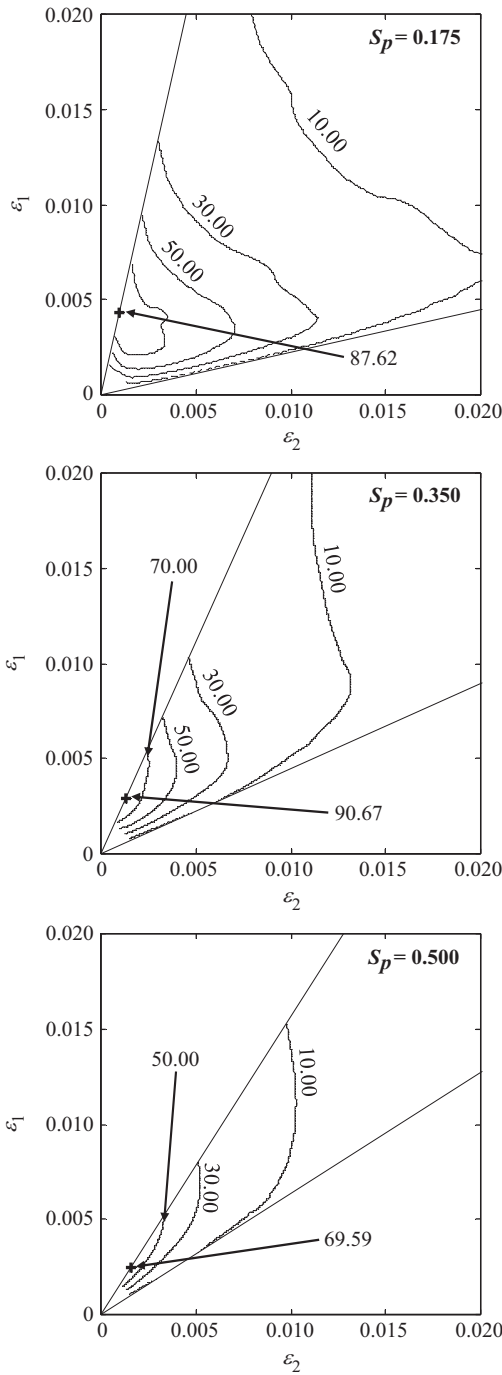


Fig. 9. Non-dimensional stiffness as a function of different texture aspect ratio combinations ϵ_1 and ϵ_2 for $S_p=0.175, 0.350$ and 0.500 , for the case of the elliptical texture shape. $\delta=0.002$ and $\lambda=2.0 \times 10^{-5}$. The optimum for each texture density is indicated by “+”. The range of combinations of ϵ_1 and ϵ_2 that constrains the dimple within the unit cell is denoted by solid lines.

ellipsoidal texture shape, for $S_p=0.175, 0.350$ and 0.500 . The optimum occurs at $S_p=0.350$ and $\epsilon_1=0.0120, \epsilon_2=0.0053$ with a minimum friction coefficient of 0.0244 , and $S_p=0.350$ and $\epsilon_1=0.0062, \epsilon_2=0.0028$ with a maximum bearing stiffness of $k=108.00$.

3.3. Chevron texture shape

An additional parameter, the area ratio K , is needed to describe the geometry of the chevron shape. K is defined as the ratio of the size of the inner equilateral triangle to that of the outer equilateral

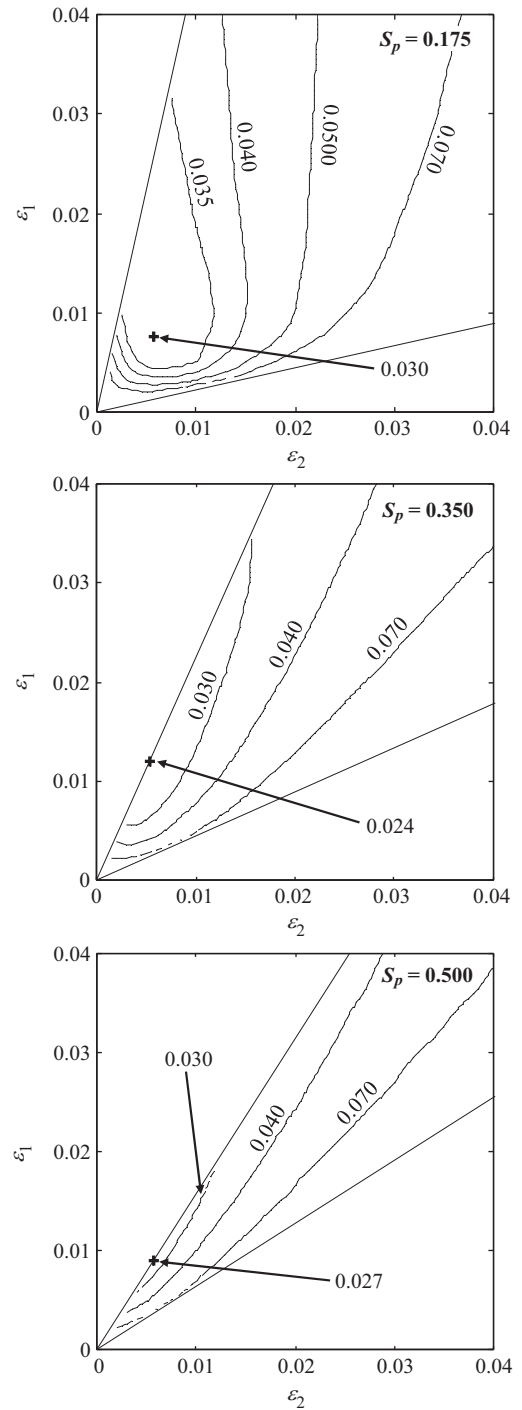


Fig. 10. Friction coefficient as a function of different texture aspect ratio combinations ϵ_1 and ϵ_2 for $S_p=0.175, 0.350$ and 0.500 , for the case of the ellipsoidal texture shape. $\delta=0.002$ and $\lambda=2.0 \times 10^{-5}$. The optimum for each texture density is indicated by “+”. The range of combinations of ϵ_1 and ϵ_2 that constrains the dimple within the unit cell is denoted by solid lines.

triangle forming the chevron shape (see Table 1). Figs. 12 and 13 display the friction coefficient and non-dimensional bearing stiffness as a function of the aspect ratio ϵ and the area ratio K , for $S_p=0.050, 0.150$ and 0.350 . Similar to the elliptical and ellipsoidal shapes, the S_p values that minimize the friction coefficient and maximize the bearing stiffness and one value on either side of that optimum are used in the analysis. The area ratio K is theoretically constrained to a value smaller than 1.0 depending on S_p , because the chevron shape cannot extend beyond the unit cell [18]. It is

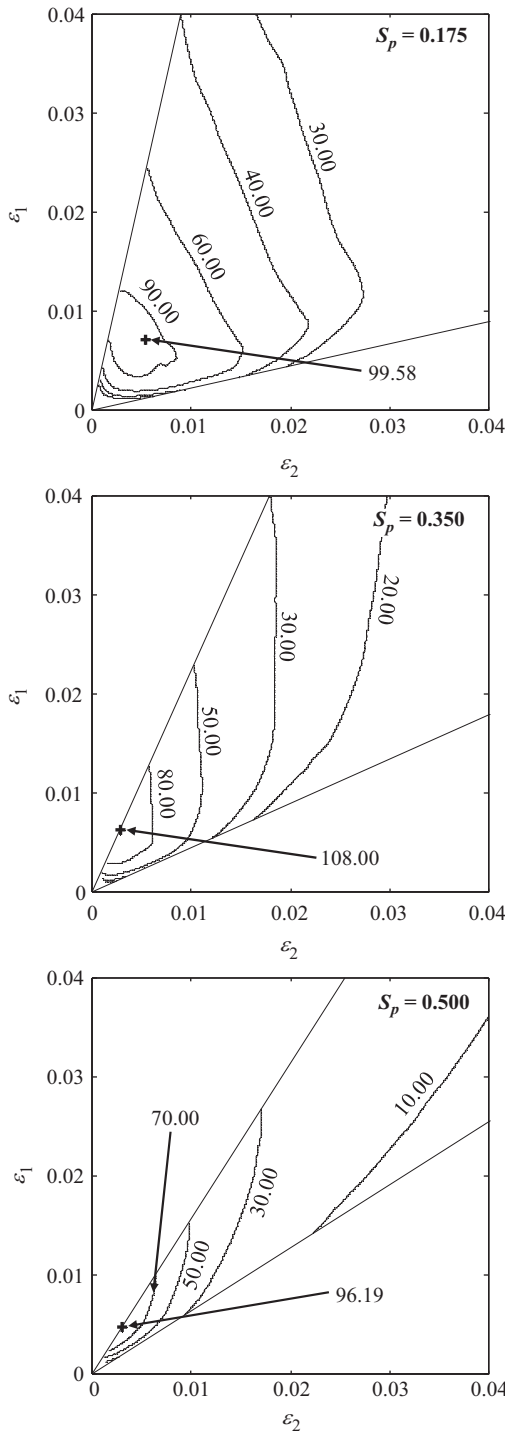


Fig. 11. Non-dimensional stiffness as a function of different texture aspect ratio combinations ϵ_1 and ϵ_2 for $S_p=0.175, 0.350$ and 0.500 , for the case of ellipsoidal texture shape. $\delta=0.002$ and $\lambda=2.0 \times 10^{-5}$. The optimum for each texture density is indicated by "+". The range of combinations of ϵ_1 and ϵ_2 that constrains the dimple within the unit cell is denoted by solid lines.

clear from Figs. 12 and 13 that the friction coefficient and the bearing stiffness change quickly with ϵ but slowly with K . Therefore, a triangular texture shape, which is a chevron texture shape with $K=0$, does not differ much from the chevron texture shape in terms of friction coefficient and bearing stiffness. This agrees with the results obtained for the load carrying capacity in [18]. However, for each S_p an optimum combination of K and ϵ exists to minimize the friction coefficient or maximize the non-dimensional bearing stiffness. The minimum friction coefficient of 0.0506

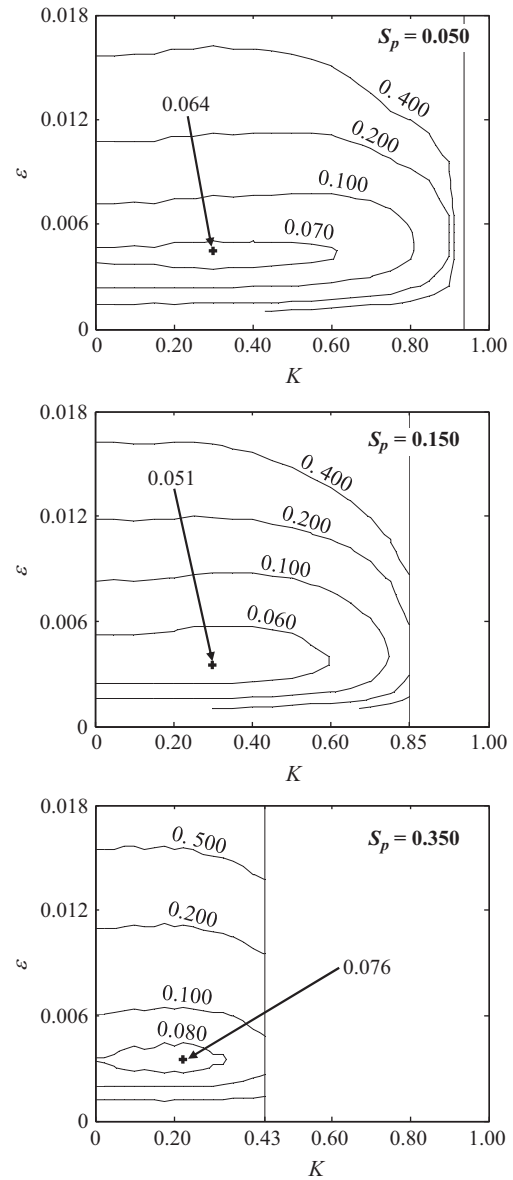


Fig. 12. Friction coefficient as a function of texture aspect ratio ϵ and area ratio K for $S_p=0.050, 0.150$ and 0.350 , for the case of the chevron texture shape. $\delta=0.002$ and $\lambda=2.0 \times 10^{-5}$. The optimum for each texture density is indicated by "+". K is limited for each S_p , denoted by the solid vertical line.

occurs for $S_p=0.150, K=0.300$, and $\epsilon=0.0035$. The maximum non-dimensional bearing stiffness is 75.86 when $S_p=0.150, K=0.250$, and $\epsilon=0.0030$.

4. Comparison of different texture shapes

Tables 2 and 3 summarize the individually optimized texture geometries for each different texture shape that result in the minimum friction coefficient and the maximum non-dimensional bearing stiffness, respectively. The difference of the friction coefficient and stiffness relative to that of the optimized spherical texture shape, which is used as a benchmark, is calculated. The minimum friction coefficient $f=0.0244$ ($\delta=0.002$ and $\lambda=2.0 \times 10^{-5}$) is obtained with the ellipsoidal texture shape, and is 24.5% lower than the friction coefficient obtained with the optimal spherical geometry, in agreement with the optimal shape for maximum load carrying capacity found in our

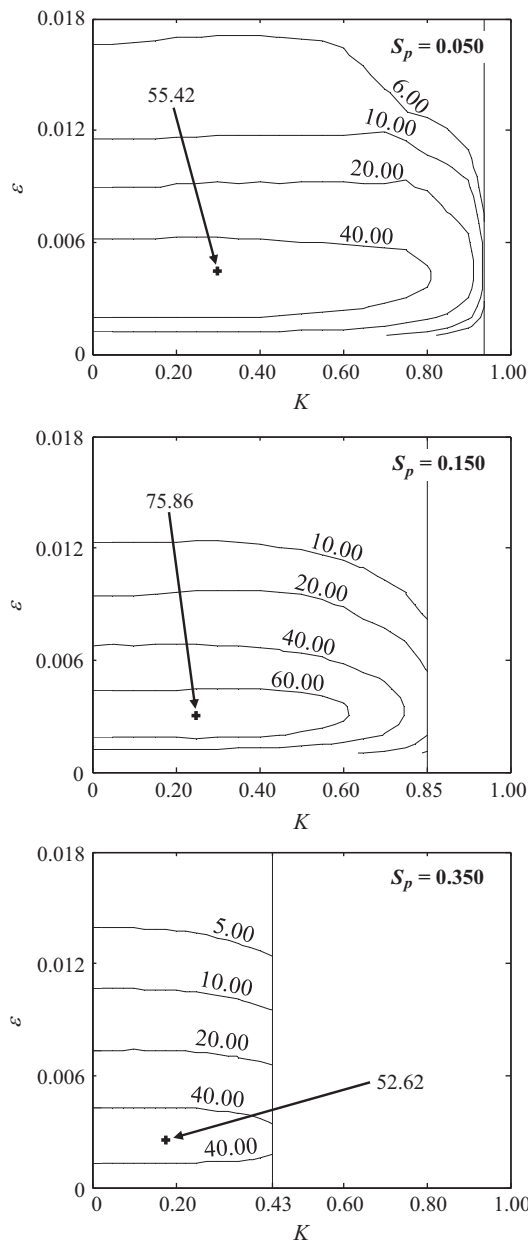


Fig. 13. Non-dimensional stiffness as a function of texture aspect ratio ϵ and area ratio K for $S_p=0.050, 0.150$ and 0.350 , for the case of the chevron texture shape. $\delta=0.002$ and $\lambda=2.0 \times 10^{-5}$. The optimum for each texture density is indicated by “+”. K is limited for each S_p , denoted by the solid vertical line.

Table 2

Optimal geometry of different texture shapes with corresponding minimized friction coefficient. The relative difference with the results for the spherical texture shape, used as a benchmark, is indicated. $\delta=0.002$ and $\lambda=2.0 \times 10^{-5}$.

Texture shape	Optimized geometry	Minimum friction coefficient	Relative friction coefficient
Circular	$S_p = 0.2000$ $\epsilon = 0.0030$	0.0371	+14.9%
Spherical	$S_p = 0.2500$ $\epsilon = 0.0050$	0.0323	0
Elliptical	$S_p = 0.3500$ $\epsilon_1 = 0.0048, \epsilon_2 = 0.0021$	0.0279	-13.6%
Ellipsoidal	$S_p = 0.3500$ $\epsilon_1 = 0.0120, \epsilon_2 = 0.0053$	0.0244	-24.5%
Triangular	$S_p = 0.1500$ $\epsilon = 0.0030$	0.0534	+65.3%
Chevron	$S_p = 0.1500$ $\epsilon = 0.0035, K = 0.3000$	0.0506	+56.7%

previous work [18]. The elliptical texture shape outperforms the spherical texture shape in terms of the minimum friction coefficient (13.6% lower). This is in contrast with the results obtained for the load carrying capacity, where the spherical texture shape outperforms the elliptical texture shape (7.8% higher) [18]. Although the elliptical texture shape reduces the load carrying capacity, the increased dimple volume also increases the equivalent spacing and, thus, reduces the shear stress compared to the spherical shape. The other differences in friction coefficient between the texture shapes correlate well with the load carrying capacity results. All texture shapes with a curved bottom profile outperform those with a flat bottom profile (spherical vs. circular, ellipsoidal vs. elliptical), and all shapes with a round edge outperform those with a straight edge/sharp angles (circular, spherical, elliptical, ellipsoidal vs. triangular and chevron). Comparing the geometries that minimize the friction coefficient of each texture shape with the geometry that maximizes the load carrying capacity [18], it is observed that a slightly higher texture density S_p and aspect ratio ϵ is required to minimize friction than to maximize the load carrying capacity. Despite the slightly sub-optimal load carrying capacity for that geometry, the increase in equivalent spacing resulting from the increased dimple volume reduces the shear stress in the bearing and, thus, reduces the friction coefficient.

The maximum bearing stiffness of the different texture shapes correlates well with the optimization results of load carrying capacity [18]. The ellipsoidal texture shape displays the maximum non-dimensional bearing stiffness of $k=108.00$, which is 9.04% higher than the benchmark spherical texture shape. Again, all texture shapes with a curved bottom profile outperform those with a flat bottom profile (spherical vs. circular, ellipsoidal vs. elliptical), and nearly all shapes with a round edge outperform those with a straight edge/sharp angles (spherical, elliptical, ellipsoidal vs. triangular and chevron). The elliptical and ellipsoidal texture shapes perform better than their symmetric counterparts (elliptical vs. circular, ellipsoidal vs. spherical) because they can be oriented perpendicular to the flow direction to maximize the effect of the texture. Interestingly, the optimal geometry of each shape that maximizes the bearing stiffness displays a higher texture density but a lower aspect ratio than the geometry that maximizes the load carrying capacity [18]. This could be clarified as follows. It is well known that the bearing stiffness decreases quickly with increasing bearing spacing [7,27]. Thus, with decreasing texture aspect ratio (a shallower dimple), the depth of the texture decreases and the bearing stiffness increases, while the load carrying capacity remains unchanged by increasing the texture density. Overall, the geometries that optimize each of the three properties; maximum load carrying capacity, minimum friction

Table 3
Optimal geometry of different texture shapes with corresponding maximized stiffness. The relative difference with the results for the spherical texture shape, used as a benchmark, is indicated. $\delta=0.002$ and $\lambda=2.0 \times 10^{-5}$.

Texture shape	Optimized geometric	Maximum non-dimensional stiffness	Relative non-dimensional stiffness
Circular	$S_p = 0.1750$ $\varepsilon = 0.0025$	74.29	-25.0%
Spherical	$S_p = 0.1750$ $\varepsilon = 0.0060$	99.05	0
Elliptical	$S_p = 0.3500$ $\varepsilon_1 = 0.0029, \varepsilon_2 = 0.0013$	90.67	-8.5%
Ellipsoidal	$S_p = 0.3500$ $\varepsilon_1 = 0.0062, \varepsilon_2 = 0.0028$	108.00	+9.0%
Triangular	$S_p = 0.1500$ $\varepsilon = 0.0030$	74.65	-24.6%
Chevron	$S_p = 0.1500$ $\varepsilon = 0.0030, K = 0.250$	75.86	-23.4%

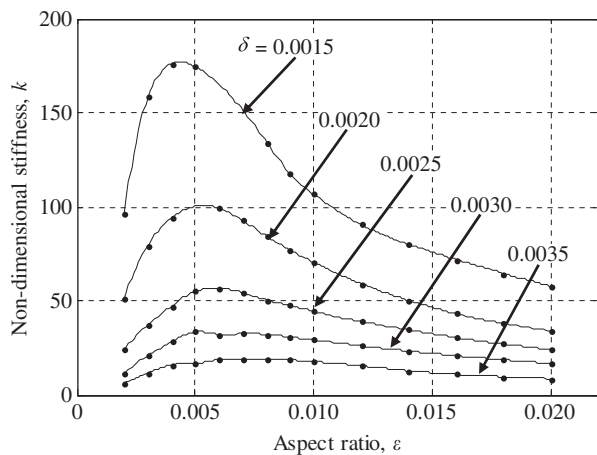


Fig. 14. Non-dimensional stiffness as a function of texture aspect ratio for different values of the non-dimensional bearing spacing, for the case of the spherical texture shape. $S_p=0.175$ and $\lambda=2.0 \times 10^{-5}$.

coefficient and maximum bearing stiffness are similar but not identical, consistent with the conclusion of [25].

As demonstrated in [18], the geometry (for each shape) that maximizes the load carrying capacity is almost independent of operating conditions (δ and λ). Similarly, the geometries that minimize the friction coefficient and maximize the bearing stiffness are almost independent of the operating conditions. As an example, Fig. 14 shows the non-dimensional stiffness k for the spherical texture shape, as a function of the aspect ratio ε , for different values of the non-dimensional spacing δ , and for $S_p=0.175$ and $\lambda=2.0 \times 10^{-5}$. Within the range of δ -values considered in this study, the aspect ratio to maximize stiffness is around 0.005 and is independent of δ .

5. Conclusion

We have optimized the geometry of six commonly used texture shapes in terms of minimizing friction coefficient and maximizing bearing stiffness of a textured parallel slider bearing with a compressible lubricant. The geometry of each texture shape is optimized independently without constraints and the optimized geometries are compared relative to each other.

(1) For each texture shape a similar, but not identical optimal texture geometry exists to minimize the friction coefficient and maximize the bearing stiffness, respectively. Additionally,

these geometries are also slightly different from the geometry that maximizes the load carrying capacity.

- (2) Texture shapes with a round edge and/or a curved bottom profile perform better than those with a straight edge or a flat bottom profile, both in minimizing the friction coefficient and maximizing the bearing stiffness.
- (3) The optimized geometries of the ellipsoidal texture shape result in the lowest friction coefficient and the highest bearing stiffness. The optimal texture density is 35% in both cases. The minimum friction coefficient is 0.0244, 24.5% lower than the optimized spherical shape, with $\varepsilon_1=0.0120$ and $\varepsilon_2=0.0053$. The maximum stiffness is 108.00, 9.0% higher than the optimized spherical shape, with $\varepsilon_1=0.0062$ and $\varepsilon_2=0.0028$.
- (4) In engineering practice, an ellipsoidal texture shape should be considered if high bearing performance is desired, in particular when a low friction coefficient is crucial, for instance to conserve energy. However, a spherical texture shape may be more cost-effective in terms of manufacturing. Finally, in applications where isotropic bearing performance is essential, i.e., the bearing performance must be independent of the sliding direction, the spherical texture shape should be considered.

Acknowledgements

This work was partially funded through National Science Foundation award #1227869. Bret Minson acknowledges support from the Undergraduate Research Opportunity Program (UROP) at the University of Utah.

Appendix A. Texture shapes and geometries

Six different texture shapes are considered in this study. The shapes, parameters and equations to describe their geometry are shown in Fig. A1 [18]. Eqs. (A.1a)–(A.1f) describe the non-dimensional spacing $H(X,Y)$ between the textured and the flat surface within one unit cell for the circular, elliptical, spherical, ellipsoidal, triangular, and chevron texture shape, respectively [18]. The circular (Fig. A1a, Eq. (A.1a)) and elliptical (Fig. A1b, Eq. (A.1b)) texture shapes are cylindrical dimples with a flat bottom profile and circular and elliptical cross-sections, respectively. The ellipsoidal texture shape is defined by a segment of an oblate ellipsoid of revolution, symmetric with respect to the flow direction (Fig. A1d, Eq. (A.1d)). A special case of the ellipsoidal texture shape is the spherical shape, featuring an isotropic configuration Fig. A1c, Eq. (A.1c). Both the elliptical and ellipsoidal texture

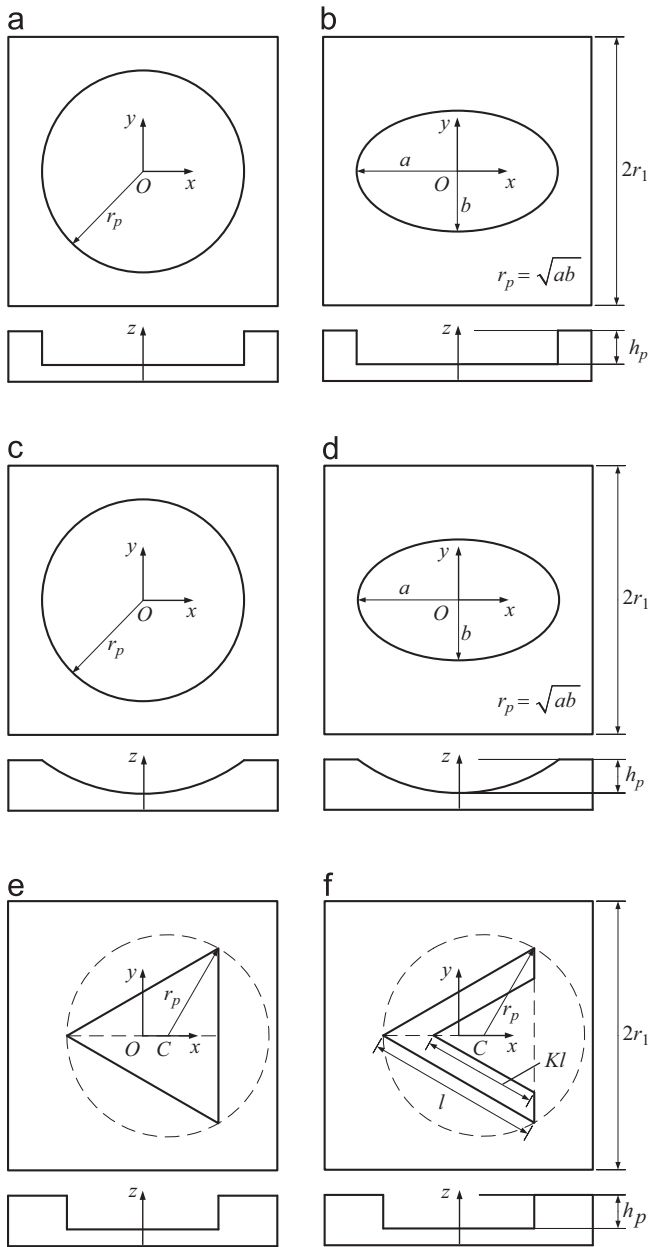


Fig. A1. Different texture shapes: (a) circle, (b) ellipse, (c) sphere, (d) ellipsoid, (e) triangle, (f) chevron. The flow is along the positive x-direction.

shapes require two aspect ratios for the eccentricity of the elliptical cross-section. The chevron texture shape consists of two similar equilateral triangles of different sizes and a flat bottom (Fig. A1f, Eq. (A.1f)). The ratio of the size of the inner triangle to that of the outer one is defined as the area ratio K . The triangular texture shape is a special case with the inner edge length of the chevron reduced to zero (Fig. A1e, Eq. (A.1e)). The circular, elliptical, spherical and ellipsoidal texture shapes all have a well-defined center which is positioned at the center of the square unit cell, which coincides with the midpoint of the altitude line of the (outer) triangle for the triangular and chevron texture shapes. This allows achieving a higher texture density for the latter two shapes. No orientation effect of the anisotropic (elliptical, ellipsoidal, triangular, chevron) textures is investigated.

$$H(X, Y) = \begin{cases} 1, & \text{if } X^2 + Y^2 > 1 \\ 1 + \frac{\varepsilon}{\delta}, & \text{if } X^2 + Y^2 \leq 1 \end{cases} \quad (\text{A.1a})$$

$$H(X, Y) = \begin{cases} 1, & \text{if } \frac{\varepsilon_1}{\varepsilon_2} X^2 + \frac{\varepsilon_2}{\varepsilon_1} Y^2 > 1 \\ 1 + \frac{\sqrt{\varepsilon_1 \varepsilon_2}}{\delta}, & \text{if } \frac{\varepsilon_1}{\varepsilon_2} X^2 + \frac{\varepsilon_2}{\varepsilon_1} Y^2 \leq 1 \end{cases} \quad (\text{A.1b})$$

$$H(X, Y) = \begin{cases} 1, & \text{if } X^2 + Y^2 > 1 \\ 1 + \frac{1}{2\delta} \sqrt{\left(\varepsilon + \frac{1}{4\varepsilon}\right)^2 - (X^2 + Y^2)} - \frac{1}{2\delta} \left(\frac{1}{4\varepsilon} - \varepsilon\right), & \text{if } X^2 + Y^2 \leq 1 \end{cases} \quad (\text{A.1c})$$

$$H(X, Y) = \begin{cases} 1, & \text{if } \frac{\varepsilon_1}{\varepsilon_2} X^2 + \frac{\varepsilon_2}{\varepsilon_1} Y^2 > 1 \\ 1 + \frac{1}{2\delta} \sqrt{\frac{\varepsilon_1}{\varepsilon_2} \left(\varepsilon_2 + \frac{1}{4\varepsilon_2}\right)^2 - \frac{\varepsilon_1}{\varepsilon_2} X^2 - \frac{\varepsilon_2}{\varepsilon_1} Y^2} - \frac{1}{2\delta} \sqrt{\frac{\varepsilon_1}{\varepsilon_2} \left(\frac{1}{4\varepsilon_2} - \varepsilon_2\right)}, & \text{if } \frac{\varepsilon_1}{\varepsilon_2} X^2 + \frac{\varepsilon_2}{\varepsilon_1} Y^2 \leq 1 \end{cases} \quad (\text{A.1d})$$

$$H(X, Y) = \begin{cases} 1, & \text{if } (X, Y) \notin \Omega \\ 1 + \frac{\varepsilon}{\delta}, & \text{if } (X, Y) \in \Omega \end{cases} \quad (\text{A.1e})$$

$$\Omega : -\frac{3}{4} \leq X \leq \frac{3}{4} \text{ and } -\frac{1}{\sqrt{3}} X - \frac{\sqrt{3}}{4} \leq Y \leq \frac{1}{\sqrt{3}} X + \frac{\sqrt{3}}{4}$$

$$H(X, Y) = \begin{cases} 1, & \text{if } (X, Y) \notin \Omega \\ 1 + \frac{\varepsilon}{\delta}, & \text{if } (X, Y) \in \Omega \end{cases} \quad (\text{A.1f})$$

$$\Omega : -\frac{3}{4} \leq X \leq \frac{3}{4} \text{ and } \begin{cases} \frac{1}{\sqrt{3}} X + \frac{\sqrt{3}}{2} (K - \frac{1}{2}) \leq Y \leq \frac{1}{\sqrt{3}} X + \frac{\sqrt{3}}{4}, & \text{if } Y \geq 0 \\ -\frac{1}{\sqrt{3}} X - \frac{\sqrt{3}}{4} \leq Y \leq -\frac{1}{\sqrt{3}} X + \frac{\sqrt{3}}{2} (\frac{1}{2} - K), & \text{if } Y \leq 0 \end{cases}$$

References

- [1] Schneider YG. Formation of surfaces with uniform micropatterns on precision machine and instruments parts. *Precision Engineering* 1984;6:219–25.
- [2] Wang X, Kato K. Improving the anti-seizure ability of SiC seal in water with RIE texturing. *Tribology Letters* 2003;14:275–80.
- [3] Wakuda M, Yamauchi Y, Kanzaki S, Yasuda Y. Effect of surface texturing on friction reduction between ceramic and steel materials under lubricated sliding contact. *Wear* 2003;254:356–63.
- [4] Stephens LS, Siripuram R, Hayden M, McCartt B. Deterministic micro asperities on bearings and seals using a modified LIGA process. *Journal of Engineering for Gas Turbines and Power* 2004;126:147–54.
- [5] Greco A, Raphaelson S, Ehmann K, Wang QJ. Surface texturing on tribological interfaces using the vibromechanical texturing method. *Journal of Manufacturing Science and Engineering—Transactions of the ASME* 2009;131:1–8.
- [6] Etsion I. State of the art in laser surface texturing. *Journal of Tribology—Transactions of the ASME* 2005;248–53.
- [7] Etsion I. Improving tribological performance of mechanical components by laser surface texturing. *Tribology Letters* 2004;17:733–7.
- [8] Feldman Y, Kligerman Y, Etsion I. A hydrostatic laser surface textured gas seal. *Tribology Letters* 2006;22:21–8.
- [9] Kligerman Y, Etsion I. Analysis of the hydrodynamic effects in a surface textured circumferential gas seal. *Tribology Transactions* 2001;44:472–8.
- [10] Brizmer V, Kligerman Y, Etsion I. A laser surface textured parallel thrust bearing. *Tribology Transactions* 2003;46:397–403.
- [11] Etsion I, Halperin G, Brizmer V, Kligerman Y. Experimental investigation of laser surface textured parallel thrust bearings. *Tribology Letters* 2004;17:295–300.
- [12] Lu X, Khonsari MM. An experimental investigation of dimple effect on the Stribeck curve of journal bearings. *Tribology Letters* 2007;27:169–76.
- [13] Ronen A, Etsion I, Kligerman Y. Friction-reducing surface-texturing in reciprocating automotive components. *Tribology Transactions* 2001;44:359–66.
- [14] Raeymaekers B, Etsion I, Talke FE. Enhancing tribological performance of the magnetic tape/guide interface by laser surface texturing. *Tribology Letters* 2007;27:89–95.
- [15] Raeymaekers B, Etsion I, Talke FE. A model for magnetic tape/guide friction reduction by laser surface texturing. *Tribology Letters* 2007;28:9–17.
- [16] Hoppermann A, Kordt M. Tribological optimisation using laser-structured contact surfaces. *O+P Oelhydraulik und Pneumatik* 2002;46:1–23.
- [17] Yu H, Wang X, Zhou F. Geometric shape effects of surface texture on the generation of hydrodynamic pressure between conformal contacting surfaces. *Tribology Letters* 2010;37:123–30.

- [18] Qiu M, Delic A, Raeymaekers B. The effect of texture shape on the load-carrying capacity of gas-lubricated parallel slider bearings. *Tribology Letters* 2012;48:315–27.
- [19] Nakano M, Korenaga A, Miyake K, Murakami T, Ando Y, et al. Applying micro-texture to cast iron surfaces to reduce the friction coefficient under lubricated conditions. *Tribology Letters* 2007;28:131–7.
- [20] Galda L, Pawlus P, Sep J. Dimples shape and distribution effect on characteristics of Stribeck curve. *Tribology International* 2009;42:1505–12.
- [21] Cupillard S, Glavatskih S, Cervantes MJ. Computational fluid dynamics analysis of a journal bearing with surface texturing. *Proceedings of the Institution of Mechanical Engineers Part J Journal of Engineering Tribology* 2008;222:97–107.
- [22] Dobrica MB, Fillon M, Pascovici MD, Cicone T. Optimizing surface texture for hydrodynamic lubricated contacts using a mass-conserving numerical approach. *Proceedings of the Institution of Mechanical Engineers Part J Journal of Engineering Tribology* 2010;224:737–50.
- [23] Ma C, Zhu H. An optimum design model for textured surface with elliptical-shaped dimples under hydrodynamic lubrication. *Tribology International* 2011;44:987–95.
- [24] Sahlin F, Glavatskih SB, Almqvist T, Larsson R. Two-dimensional CFD-analysis of micro-patterned surfaces in hydrodynamic lubrication. *Journal of Tribology—Transactions of the ASME* 2005;127:96–102.
- [25] Pascovici MD, Cicone T, Fillon M, Dobrica MB. Analytical investigation of a partially textured parallel slider. *Proceedings of the Institution of Mechanical Engineers Part J Journal of Engineering Tribology* 2009;223:151–8.
- [26] Siripuram RB, Stephens LS. Effect of deterministic asperity geometry on hydrodynamic lubrication. *Journal of Tribology—Transactions of the ASME*, 126; 527–34.
- [27] Murthy AN, Etsion I, Talke FE. Analysis of surface textured air bearing sliders with rarefaction effects. *Tribology Letters* 2007;28:251–61.
- [28] Feldman Y, Kligerman Y, Etsion I. Stiffness and efficiency optimization of a hydrostatic laser surface textured gas seal. *Journal of Tribology—Transactions of the ASME*, 129; 407–10.
- [29] Raeymaekers B, Etsion I, Talke FE. The influence of operating and design parameters on the magnetic tape/guide friction coefficient. *Tribology Letters* 2006;25:161–71.